

Two-Step Image Dehazing with Intra-domain and Inter-domain Adaption

Xin Yi, Bo Ma[†], Yulin Zhang, Longyao Liu, JiaHao Wu

Abstract—Recently, image dehazing task has achieved remarkable progress by convolutional neural network. However, those approaches mostly treat haze removal as a one-to-one problem and ignore the intra-domain gap. Therefore, haze distribution shift of the same scene images is not handled well. Also, dehazing models trained on the labeled synthetic datasets mostly suffer from performance degradation when tested on the unlabeled real datasets due to the inter-domain gap. Although some previous works apply translation network to bridge the synthetic domain and the real domain, the intra-domain gap still exists and affects the inter-domain adaption. In this work, we propose a novel Two-Step Dehazing Network (TSDN) to minimize the intra-domain gap and the inter-domain gap. First, we propose a multi-to-one dehazing network to eliminate the haze distribution shift of images within the synthetic domain. Then, we conduct an inter-domain adaption between the synthetic domain and the real domain based on the aligned synthetic features. Extensive experimental results demonstrate that our framework performs favorably against the state-of-the-art algorithms both on the synthetic datasets and the real datasets.

Index Terms—Image dehazing, intra-domain adaption, inter-domain adaption.

I. INTRODUCTION

IMAGE dehazing task aims to recover the clear images from their corresponding hazy images. The whole procedure can be formulated as

$$I(x) = J(x)t(x) + A(1 - t(x)) \quad (1)$$

where $I(x)$ denotes the hazy image and $J(x)$ denotes the clear image, x denotes a pixel position in the image, A denotes the global atmospheric light and $t(x)$ denotes the transmission map. In homogeneous situation, the transmission map can be represented as $t(x) = e^{-\beta d(x)}$, where β and $d(x)$ is the atmosphere scattering parameter and the scene depth, respectively.

Obviously, image dehazing is an ill-posed problem. So, many researchers try to transform this problem into a well-posed problem by estimating the atmospheric light intensity and the transmission map via certain priors [2], [3], [4]. However, those methods are not robust and tend to fail in some scene, especially where the color of objects are similar to the atmospheric light. More recently, to avoid hand-craft priors, other researchers apply convolutional neural network to directly predict the transmission map and the atmospheric light intensity from training data [5], [6], [7]. However, those



(a) Input (b) MSBDN-DFF [1] (c) Ours

Fig. 1: The dehazed results of the same scene images with haze distribution shift. Our method generates cleaner images than MSBDN-DFF. More importantly, our method avoids performance gap when faced with the intra-domain gap. (a) Hazy images. (b) Results of MSBDN-DFF. (c) Our results.

methods split the whole dehazing framework into two parts, without considering the inherent connection between them. In addition, inaccurate estimation of the transmission map and the atmospheric light intensity would lead to undesirable results.

To overcome those problems, the end-to-end dehazing frameworks [8], [9], [10], [1] are proposed to predict clear images directly from hazy inputs. However, those methods mainly focus on the one-to-one dehazing task, i.e., dehazed result is generated by a single hazy image. The intra-domain gap that haze distribution shift among hazy images of the same scene receives little attention. Therefore, when the haze distribution changes, the performance of those methods will change simultaneously. As shown in Figure 1, MSBDN-DFF [1] suffers from performance drop due to the intra-domain gap. In addition, previous approaches mostly train models on the labeled synthetic datasets because it is difficult to obtain sufficient hazy images with ground truth in real world. Naturally, those approaches perform poorly on real hazy images due to the inter-domain gap. To address this issue, Shao et al. [11] attempt to bridge the synthetic domain and the real domain by applying bidirectional translation

The authors are with the Beijing Laboratory of Intelligent Information Technology, School of Computer Science and Technology, Beijing Institute of Technology, Beijing 100081, China.

[†]Corresponding author.

network. Nevertheless, they only deal with the inter-domain gap between the synthetic domain and the real domain while ignoring the intra-domain gap.

In order to improve the robustness of the model under different haze distributions and the generalization under different domains, we propose a two-step image dehazing network (TSDN), which comprises an intra-domain adaption step and an inter-domain adaption step. First, we extract features of hazy images which are in the same scene but with different haze distributions. Then, we pick the base feature according to loss-based deep supervision and align other features to the base feature. Thus, the distribution shift of images within the synthetic domain is eliminated in the feature space. Finally, we apply the similar alignment in the inter-domain adaption step to close the inter-domain gap. For image dehazing on synthetic datasets and real datasets, our proposed framework achieves state-of-the-art performance against previous algorithms. The contributions of this work are summarized as follows:

- We propose a novel intra-domain adaption on feature layer which closes the haze distribution gap of the same scene images.
- We propose an inter-domain adaption for image dehazing on the real hazy images based on the aligned intra-domain features.
- We conduct extensive experiments and comprehensive ablation studies on the synthetic datasets and the real datasets which validate the effectiveness of our proposed method.
- Our domain adaption module can be integrated into existing dehazing frameworks for performance improvement.

II. RELATED WORKS

In this section, we briefly review the image dehazing, domain adaption and deeply-supervised learning methods, which are related to our work.

A. Image Dehazing

Previous image dehazing approaches can be divided into two mainstreams, where one is based on prior and the other is based on learning.

1) *Prior-based methods*: Those methods recover clear images through statistics prior, e.g., the albedo of the scene in [12]. Recently, researchers have explored different priors for image dehazing [2], [3], [13], [4]. Specifically, based on the observation that clear images have higher contrast than hazy images, Tan et al. [2] enhance the visibility of hazy images by maximizing local contrast. He [3] proposes dark channel prior (DCP) that the intensity of pixels in haze-free patches is very low in at least one color channel to achieve image dehazing. Besides, based on a generic regularity that small image patches typically exhibit a one-dimensional distribution in the RGB color space, Fattal [13] proposes a color-lines approach to recover the scene transmission. Zhu et al. [4] propose color attenuation prior to recover the scene depth of the hazy image with a supervised learning method.

All above methods heavily rely on hypothetical priors. However, those priors tend to lose effectiveness in complex scene, leading to performance drop.

2) *Learning-based methods*: Different from the above methods, learning-based methods use convolutional neural networks to recover clear images from hazy images directly [5], [14], [8], [9], [10], [11], [1]. Specifically, an end-to-end system for transmission estimation is proposed in [5]. Ren et al. [14] design a multi-scale neural network for learning transmission maps from hazy images in a coarse-to-fine manner. Qiu et al. [9] propose a pix2pix model with an enhancer block which reinforces the dehazing effect in both color and details. A multi-scale boosted decoder with dense feature fusion is proposed to restore clear images in [1]. However, those methods only focus on the one-to-one image dehazing while ignores the intra-domain gap.

B. Domain Adaption

The purpose of domain adaption is to eliminate the distribution difference between labeled source domain and target domain. Recently, numerous domain adaption approaches have been proposed, including aligning the source domain and target domain distributions, generating a mapping between two domains, or creating ensemble models [15]. The alignment based methods can be divided into pixel-level alignment [16], [17], [18], [19], [20] and feature-level alignment [21], [22], [23]. The feature-level alignment methods mostly try to produce feature maps with the same distribution from images with different distributions. And the pixel-level alignment methods usually learn a transformation in the pixel space from one domain to the other [16].

With the introduction of GAN [24], adversarial learning begins to be used in other computer vision tasks, e.g., image generation [25], [26], [27], image-to-image translation [18], [28], [29], [30], etc. Among them, adversarial-based unsupervised domain adaption (UDA) utilizes adversarial learning to learn domain invariant features. This framework usually consists of a generator and a discriminator, where they play min-max games to obtain the distribution migration from the source domain to the target domain.

In image dehazing field, Shao et al. [11] propose a bidirectional translation network to bridge the domain gap. However, they only consider the inter-domain gap. In this work, we further minimize the intra-domain gap to achieve extra performance gains.

C. Deeply Supervised Learning

The deeply supervised learning is proposed in [31]. They apply the classifier on the deep feature layers of the neural networks to promote better convergence. Also, they draw a conclusion that more discriminative features will improve the final performance of the classifier. Recently, the deeply supervised learning is widely used in image classification [32], semantic segmentation [33], human pose estimation [34].

In this work, we append auxiliary supervision branch on the feature layer. Unlike classification tasks which want to make features more discriminative, we want to make features of the same scene images less discriminative, i.e., eliminating haze distribution shift in feature space. Furthermore, our supervised learning is based on the dehazing loss so that we can ensure all features are aligned to the best one.

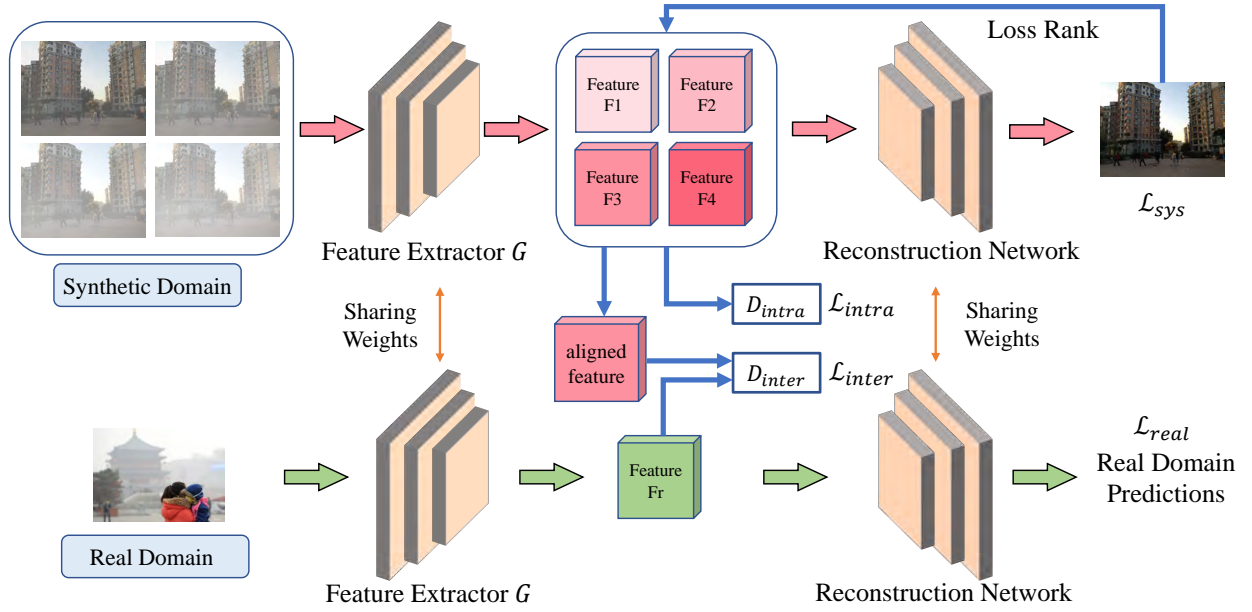


Fig. 2: Illustration of our proposed method. The overall framework consists of two main modules, the dehazing module and the domain adaption module. The dehazing module that comprises a feature extractor G and a reconstruction network aims to recover clear images from hazy images as depicted by red arrows and green arrows. The domain adaption module is divided into two steps, intra-domain adaption and inter-domain adaption, aiming to close the intra-domain gap and the inter-domain gap. In intra-domain phase, we propose a loss-based deep supervision and an intra-domain feature alignment to eliminate haze distribution shift of the same scene images. In inter-domain phase, we apply inter-domain feature alignment based on the aligned synthetic feature to close the inter-domain gap.

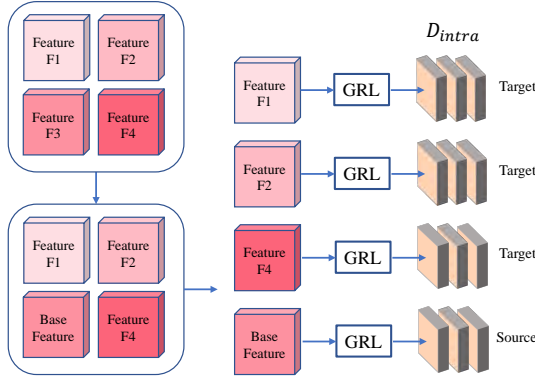


Fig. 3: Illustration of the intra-domain adaption. First, we apply loss-based deep supervision to select the base feature F_b from all features of the same scene images. Then, we align all other features to the base feature in order to eliminate haze distribution shift. This alignment is achieved by the intra-domain discriminator D_{intra} and the GRL [35] module, where D_{intra} tries to distinguish F_b and GRL module reverses the gradient so that feature extractor G will generate similarly distributed features to confuse D_{intra} .

III. METHOD

In this section, we introduce our overall method in section III-A, intra-domain adaption in section III-B, inter-domain adaption in section III-C and loss functions in section III-D.

A. Method Overview

The overall framework comprises a dehazing module and a domain adaption module which is illustrated in Figure 2. The goal of the dehazing module is to recover clear images from hazy images and the goal of the domain adaption module is to achieve intra-domain adaption and inter-domain adaption. We first minimize the intra-domain gap then the inter-domain gap. In the intra-domain phase, we take a set of hazy images in the same scene but with different haze distributions as input and get their corresponding features by the feature extractor G . We align all other features to the base feature F_b by the intra-domain discriminator D_{intra} . In the inter-domain phase, we take real hazy images and synthetic hazy images as input and get their features by the same feature extractor G . We align real domain features to synthetic domain features through the inter-domain discriminator D_{inter} .

B. Intra-domain Adaption

Generally, a clear image corresponds to multiple hazy images with different haze distributions. The goal of intra-domain adaption is to align those hazy images and improve the performance on each image. To this end, we apply adversarial alignment in feature space via intra-domain discriminator D_{intra} .

Suppose we have n hazy images $\{x_i \in \mathbb{R}^{H \times W \times 3}\}_{i=1}^n$ that belong to the same scene, we can extract n features $\{F_i \in \mathbb{R}^{h \times w \times k}\}_{i=1}^n$ with a designed feature extractor network G . To find the base feature F_b to which all other features

are aligned, we apply deeply supervised learning based on the dehazing loss. Specifically, we input all features into the reconstruction module to get their corresponding haze-free predictions and dehazing losses L_{sys} . According to those losses, we pick the feature with the lowest dehazing loss as base feature F_b . Then, base feature F_b along with other features F_j ($j = 1, 2, \dots, n$ and $j \neq b$) are fed into a fully-convolutional network D_{intra} to generate intra-domain classification score maps. The score map has the same spatial resolution as the feature where each pixel position represents the intra-domain prediction of the same position in the feature. The loss function between the predicted classification score map and the label is binary cross-entropy loss which can be written as

$$\mathcal{L}_{intra} = -\frac{1}{n-1} \sum_j \sum_{h,w} y \log(D_{intra}(F_b^{(h,w)})) + (1-y) \log(1 - D_{intra}(F_j^{(h,w)})) \quad (2)$$

where (h, w) denotes a pixel position in the feature and y denotes intra-domain label. In our work, we set label y of source and target as 1 and 0, respectively. Correspondingly, base feature F_b is the intra-domain source and other features F_j are the intra-domain target. For the discriminator D_{intra} , we optimize it using loss function Eq.(2). For feature extractor G , we apply gradient reversal layer (GRL) [35] to perform adversarial learning. The pipeline of the deeply supervised learning and the intra-domain adaption is illustrated in Figure 3. The discriminator D_{intra} tries to distinguish F_b from F_j ($j = 1, 2, 4$) while feature extractor G tries to generate similarly distributed F_b and F_j to confuse D_{intra} . Thus, the haze distribution shift is eliminated in feature space.

C. Inter-domain Adaption

The goal of the inter-domain adaption is to close the inter-domain gap between the synthetic domain and the real domain. In order to prevent the intra-domain alignment process from affecting the inter-domain alignment, we apply inter-domain adaption after we finish our intra-domain alignment.

We perform inter-domain adaption in feature space by adversarial learning. Particularly, given a synthetic hazy image $x_s \in \mathbb{R}^{H \times W \times 3}$ and a real hazy image $x_r \in \mathbb{R}^{H \times W \times 3}$, we extract their features $F_s \in \mathbb{R}^{h \times w \times k}$ and $F_r \in \mathbb{R}^{h \times w \times k}$ by extractor network G , respectively. Note that F_s is already aligned within the synthetic domain. Then, we obtain domain classification prediction maps of F_s and F_r by a fully-convolutional discriminator network D_{inter} . The prediction map has the same spatial shape as input and each position on it denotes domain label of the same position on input. We apply binary cross-entropy loss between the classification score map and the label which can be written as

$$\mathcal{L}_{inter} = -\sum_{h,w} z \log(D_{inter}(F_s^{(h,w)})) + (1-z) \log(1 - D_{inter}(F_r^{(h,w)})) \quad (3)$$

where (h, w) denotes a pixel position in the feature and z denotes inter-domain label. We set the synthetic domain as source and real domain as target, where source label is 1 and target label is 0.

D. Loss Functions

Given a synthetic dataset D_{sys} and a real dataset D_{real} , where D_{sys} consists of a hazy subset $I_{haze} = \{x_h\}_{h=1}^{N_h}$ and a clear subset $I_{clear} = \{x_c\}_{c=1}^{N_c}$ while D_{real} only contains a hazy set $J_{haze} = \{x_r\}_{r=1}^{N_r}$. We adopt following loss functions in our framework.

1) *Domain Adversarial Losses*: As described in section III-B and III-C, domain adversarial losses are generated by D_{intra} and D_{inter} . On the scale of the entire dataset, the intra-domain loss can be written as

$$\mathcal{L}_1 = \sum_{c=1}^{N_c} \mathcal{L}_{intra} \quad (4)$$

and the inter-domain loss can be written as

$$\mathcal{L}_2 = \sum_{i=1}^{N_i} \mathcal{L}_{inter} \quad (5)$$

where N_i denotes minimum of N_c and N_r .

2) *Image Dehazing Losses*: Those losses measure the difference between the predicted images and the ground truth. In the synthetic domain, we apply $L1$ loss to make sure the dehazed results are close to the clear images. Since a clear image corresponds to multiple hazy images, we further define the hazy subset as $I_{haze} = \{x_h^{(c)}, c = 1, 2, \dots, N_c\}_{h=1}^{N_h}$, where $x_h^{(c)}$ represents the h -th hazy image corresponding to the c -th clear image. Thus, the predicted clear images can be defined as $I_{pre} = \{y_h^{(c)}, c = 1, 2, \dots, N_c\}_{h=1}^{N_h}$. The dehazing loss between I_{pre} and I_{clear} are defined as

$$\mathcal{L}_{sys} = \frac{1}{N_h} \sum_{h=1}^{N_h} \left\| y_h^{(c)} - x_c \right\|_1 \quad (6)$$

Besides, in order to improve the performance of our model in the real domain, we add the dark channel prior loss [3] and the total variation loss on the predicted real images following Shao [11]. The dark channel prior of an image is defined as

$$I^{dark}(x) = \min_{p \in P(x)} \left(\min_{c \in \{r, g, b\}} I^c(p) \right) \quad (7)$$

where I is an image and c is a color channel of I , x represents a pixel position of I and $P(x)$ represents a local patch centered at x . We divide an image into n patches and define the overall dark channel loss as

$$\mathcal{L}_{dc} = \frac{1}{n} \sum_x \left\| I^{dark}(x) \right\|_1 \quad (8)$$

The total variation loss is defined as

$$\mathcal{L}_{tv} = \frac{1}{w} \sum_i \left\| I_{i+1,j} - I_{i,j} \right\|_1 + \frac{1}{h} \sum_j \left\| I_{i,j+1} - I_{i,j} \right\|_1 \quad (9)$$

where i and j denote the horizontal position and the vertical position of an image, respectively. w is the width of the image and h is the height. So, the image dehazing loss in the real domain can be written as

$$\mathcal{L}_{real} = \lambda_{dc} \mathcal{L}_{dc} + \lambda_{tv} \mathcal{L}_{tv} \quad (10)$$

Layer	Channels (In)	Channels (Out)	Output
Conv	3	64	-
DownSampling	64	128	-
DownSampling	128	256	-
ResBlocks-9	256	256	Feature
ResBlocks-9	256	256	-
UpSampling	256	128	-
UpSampling	128	64	-
Conv	64	3	Dehazed image

TABLE I: Configurations of dehazing module. “Conv” represents the convolution layer, “ResBlocks-9” represents 9 residual blocks.

3) *Overall Loss*: The overall loss is defined as weighted sum of all losses. In intra-domain training phase, the overall loss can be written as

$$\mathcal{L}_{altra} = \lambda_1 \mathcal{L}_1 + \lambda_3 \mathcal{L}_{sys} \quad (11)$$

while in inter-domain training phase, the overall loss can be written as

$$\mathcal{L}_{alter} = \lambda_2 \mathcal{L}_2 + \lambda_3 \mathcal{L}_{sys} + \lambda_4 \mathcal{L}_{real} \quad (12)$$

IV. EXPERIMENTS

We introduce related experiments and ablation studies in this section to verify our proposed method.

A. Experimental details

B. Datasets

We choose RESIDE [36] dataset as our training dataset. For the intra-domain adaption step, we randomly sample 8000 hazy images from ITS (Indoor Training Set) and 8000 hazy images from OTS (Outdoor Training Set). Every four hazy images correspond to one clear image, in other words, there are total 20,000 images in the synthetic training set. For the inter-domain adaption step, we randomly sample 3000 images from URHI (Unannotated Realistic Hazy Images). To achieve data augmentation, we randomly crop images to 256×256 and randomly flip the cropped images horizontally during the training phase. Furthermore, we ensure that the crop areas and horizontal directions of the same scene images (four hazy images and one clear image) are consistent in each iteration.

C. Implementation details

We implement our proposed method TSDN using PyTorch [37] framework, and we conduct experiments on both our designed network architecture (Table I) and MSBDN-DFF [1] network architecture. First, we train the dehazing module and the intra-domain discriminator within the synthetic domain for 200 epochs. For the dehazing module, we apply the SGD [38] optimizer with learning rate 1.25×10^{-4} , momentum 0.9 and weight decay 5×10^{-4} . For the intra-domain discriminator, we apply the Adam [39] optimizer with learning rate 1×10^{-4} , $\beta_1 = 0.9$ and $\beta_2 = 0.99$. We set parameter of reversed gradients as 0.1 in GRL module. For the overall loss in the intra-domain phase, we set λ_1 and λ_3 as 1.

Then, we adapt model to real hazy images by training model with inter-domain discriminator for 20 epochs. Also, we apply SGD optimizer with learning rate 1×10^{-4} for the dehazing module and Adam optimizer with learning rate 1×10^{-4} for the inter-domain discriminator. For the overall loss in the inter-domain phase, we set $\lambda_2 = 1$, $\lambda_3 = 1$, $\lambda_4 = 1$, $\lambda_{tv} = 10^{-1}$ and $\lambda_{dc} = 10^{-3}$.

D. Results on Synthetic Datasets

We evaluate our proposed framework and compare it with other previous methods on SOTS [36] dataset. The dehazed results of same scene images with haze distribution shift are shown in Figure 4. From the results, we can observe that previous algorithms all encounter the phenomenon of performance gap when facing different haze distributions, e.g., magnified area in the images. Normally, if a hazy image has thicker haze, the dehazed image has higher chance that it remains haze in global or detail. Compared with previous methods, our approach generates clearer images under different haze situations which verifies the effectiveness of the intra-domain adaption (more detailed proof can be found in IV-F).

The quantitative evaluation are shown in Table II. Our method achieves the best performance on both PSNR and SSIM. Compared with the state-of-the-art method MSBDN-DFF [1], our method achieves performance gain with 1.47dB on PSNR and 0.002 on SSIM.

E. Results on Real Images

To evaluate our method in the real domain, we conduct experiments on the real dataset RTTS [36] and compare visual results with other previous methods.

The visual results are shown in Figure 5. From the results, we can observe that previous dehazing methods have different limitations on real images. Specifically, DCP [3] suffers from serious color distortion and overexposure, e.g., the first, third and fourth rows of Figure 5 (b). Besides, the dehazed results of Dehazenet [5], FFA [10] and MSBDN-DFF [1] all have residual haze, e.g., the first, fourth and sixth rows of Figure 5 (c), (f) and (g). In addition, the dehazed results of EPDN [9] suffer from brightness issues (much darker), e.g., the third row and the traffic signs in the seventh row of Figure 5 (d) and color distortion (some results are more yellow than other methods), e.g., the sixth and seventh rows of Figure 5 (d). Furthermore, DAdehazing [11] reaches better visual results than the other previous methods. The overall brightness and the color are well-maintained during dehazing process. However, there is still some residual haze, e.g., the trees in the fourth row of Figure 5 (e). More importantly, some results of DAdehazing become less realistic or blur due to the effect of GAN, e.g., the people in the first row, the trees in the fourth row and the people in the sixth row of Figure 5 (e). Overall, the method we proposed achieves the best performance in removing haze, maintaining the color and brightness of the images, and restoring details.

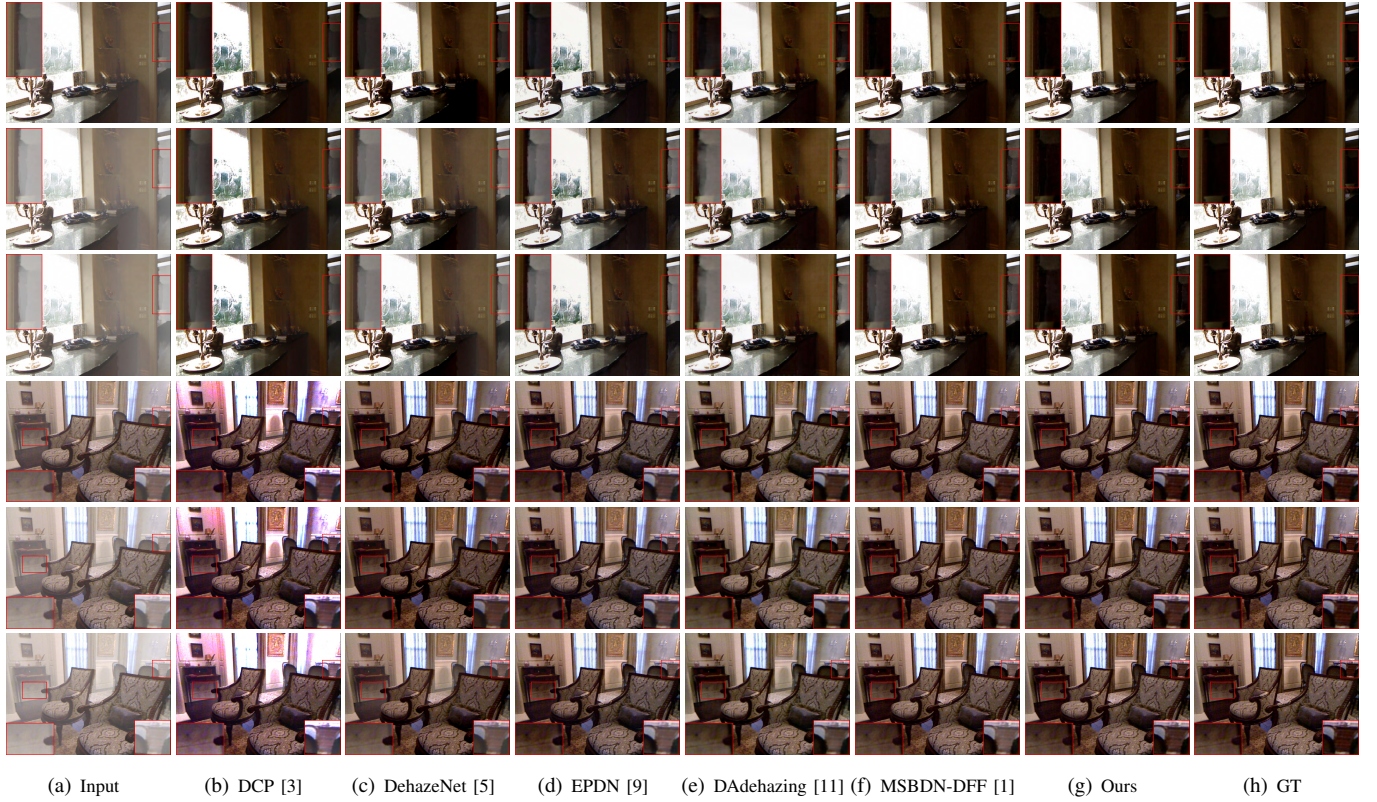


Fig. 4: Visual results of images with different haze distributions on SOTS [36] dataset

	DCP [3]	DehazeNet [5]	DCPDN [6]	EPDN [9]	GfN [40]	GDN [41]	DAdehazing [11]	MSBDN-DFF [1]	Ours
PSNR	15.49	21.14	19.39	23.82	22.30	31.51	27.76	33.79	35.26
SSIM	0.646	0.853	0.659	0.893	0.886	0.982	0.928	0.983	0.985

TABLE II: Quantitative evaluation of the dehazing results on SOTS [36] dataset.

	BS	ITA	LDS	PSNI	SSIM
SOTS	ResBlocks			23.80	0.881
	ResBlocks	✓		27.32	0.929
	ResBlocks	✓	✓	28.13	0.941
	MSBDN-DFF			33.79	0.983
	MSBDN-DFF	✓		34.45	0.984
	MSBDN-DFF	✓	✓	35.26	0.985

TABLE III: Ablation study on SOTS [36] dataset. “ITA” denotes the intra-domain adaption, “LDS” denotes the loss-based deep supervision and “ResBlocks” is the dehazing module in Table I.

F. Ablation Study

In order to verify the effectiveness of each module in our proposed method, we conduct ablation studies on the intra-domain adaption and the inter-domain adaption.

In the intra-domain adaption part, we conduct ablation study using the following settings: 1) **BS**: base network; 2) **BS+ITA**: base network with the intra-domain adaption; 3) **BS+ITA+LDS**: base network with the intra-domain adaption

and the loss-based deep supervision.

The quantitative results of the intra-domain adaption are shown in Table III, which demonstrates that base network with the intra-domain adaption and the loss-based deep supervision achieves the best performance. To further prove that the improvement on performance is promoted by the intra-domain adaption, we compare the intra-domain gap under all three methods. Instead of directly measuring the distribution similarity of the features which is not intuitive, we utilize dehazing losses to measure the intra-domain gap. In other words, if the dehazing losses of the same scene are less discrete, the features of the same scene are more closely aligned. Specifically, we calculate the range, the standard deviation and the coefficient of variation of the dehazing losses in each scene and take the average of all scenes. The results are shown in Figure 6. From the results, we can observe that dehazing losses decrease faster after we apply the intra-domain adaption to base network. Moreover, dehazing losses are more compact in methods with the intra-domain adaption which demonstrates that the features of the same scene images are aligned in feature space.

In the inter-domain part, we conduct ablation study with the following settings: 1) **BS**: base network; 2) **BS+ITE**: base

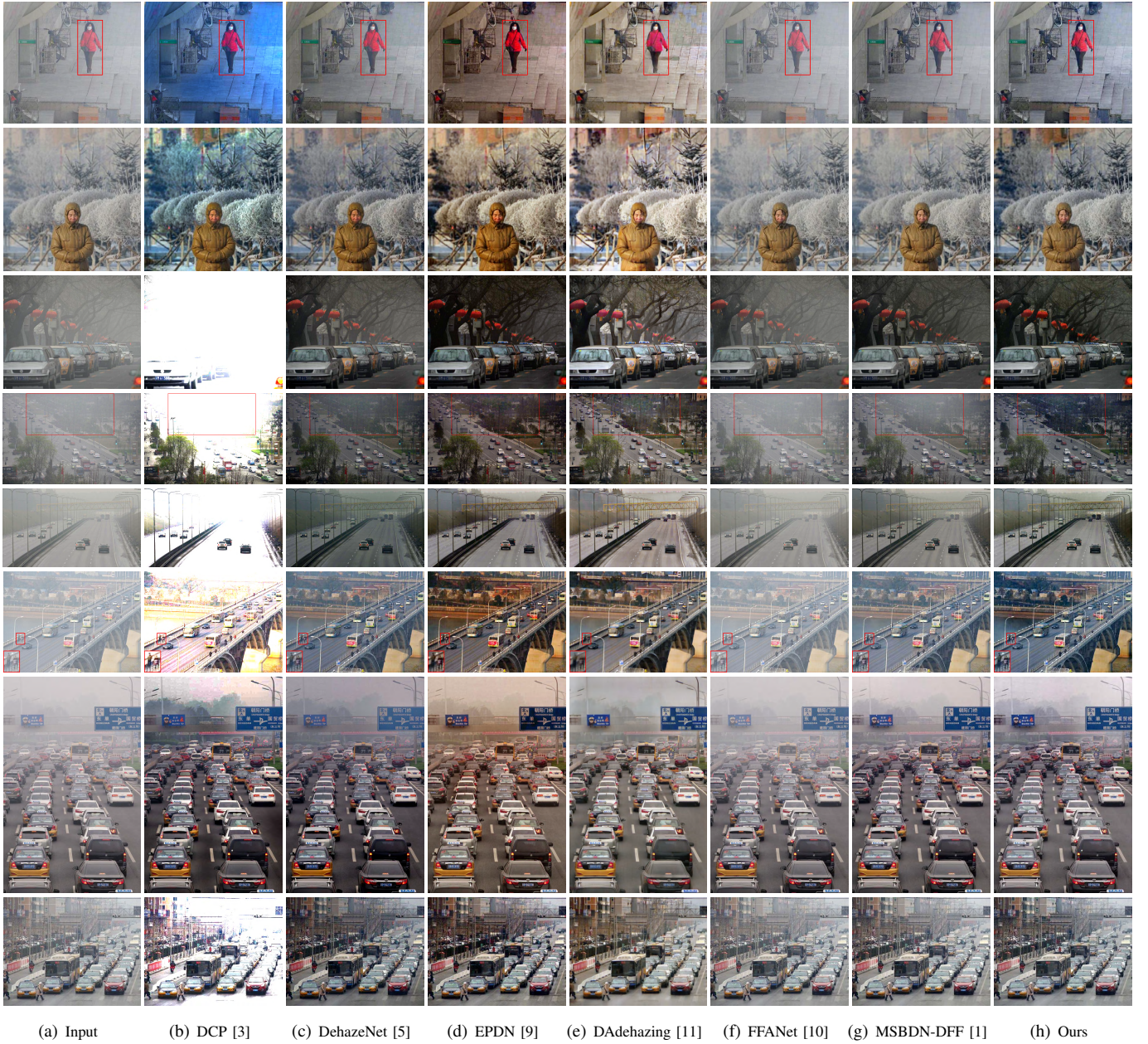


Fig. 5: Visual results of real world hazy images on RTTS [36] dataset

network with the inter-domain adaption; 3) **BS+ITA**: base network with the intra-domain adaption; 4) **BS+ITA+ITE**: base network with the intra-domain and the inter-domain adaption.

The visual results are shown in Figure 7. The result of base network has residual haze due to the domain gap. This phenomenon is alleviated by the intra-domain adaption or the inter-domain adaption. However, color distortion appears if the inter-domain adaption is directly applied because the network is sensitive to the haze distribution of the input image. Base network with intra-domain adaption and inter-domain adaption achieve the best performance.

V. CONCLUSION

In this paper, we propose a novel two-step dehazing network (TSDN) which consists of an intra-domain adaption step and an inter-domain adaption step. First, we apply the intra-domain adaption within the synthetic domain by adversarial learning and deeply supervised learning. Specifically, we extract features of the same scene images with different haze distributions and seek base feature from those features by dehazing loss. Then, we align other features to the base feature to eliminate distribution difference of input images. Furthermore, we apply the inter-domain adaption between the synthetic domain and the real domain based on the aligned synthetic features. Our proposed methods can be easily integrated into existing dehazing frameworks. Extensive experimental results demonstrate

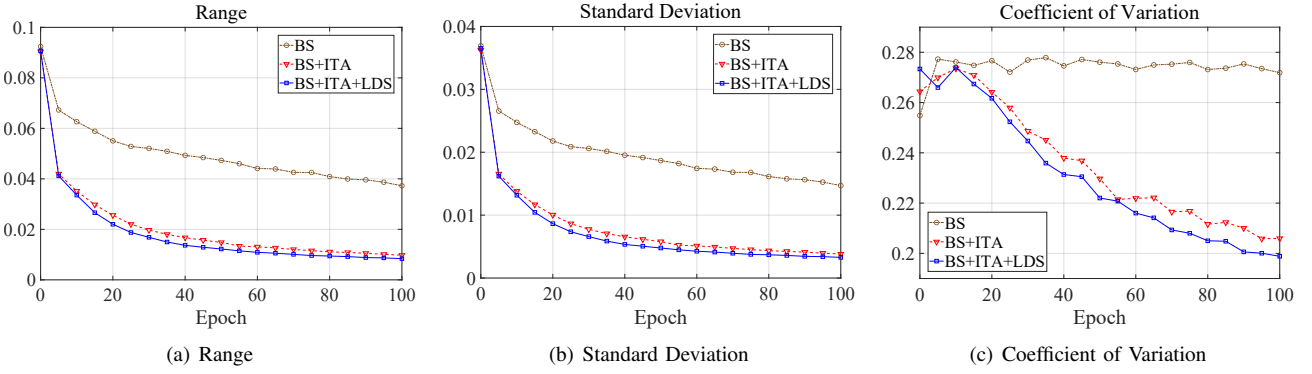


Fig. 6: The dispersion evaluation of the dehazing losses. Network with the intra-domain adaption gets more compact dehazing losses which demonstrates that the features are aligned in feature space.



Fig. 7: Ablation study of real world hazy images on RTTS [36] dataset.

that our method perform favorably against the state-of-the-art algorithms both on the synthetic datasets and the real datasets.

REFERENCES

- [1] H. Dong, J. Pan, L. Xiang, Z. Hu, X. Zhang, F. Wang, and M.-H. Yang, "Multi-scale boosted dehazing network with dense feature fusion," in *Proceedings of the IEEE/CVF Conference on Computer Vision and Pattern Recognition*, 2020, pp. 2157–2167.
- [2] R. T. Tan, "Visibility in bad weather from a single image," in *2008 IEEE Conference on Computer Vision and Pattern Recognition*. IEEE, 2008, pp. 1–8.
- [3] K. He, J. Sun, and X. Tang, "Single image haze removal using dark channel prior," *IEEE transactions on pattern analysis and machine intelligence*, vol. 33, no. 12, pp. 2341–2353, 2010.
- [4] Q. Zhu, J. Mai, and L. Shao, "A fast single image haze removal algorithm using color attenuation prior," *IEEE transactions on image processing*, vol. 24, no. 11, pp. 3522–3533, 2015.
- [5] B. Cai, X. Xu, K. Jia, C. Qing, and D. Tao, "Dehazenet: An end-to-end system for single image haze removal," *IEEE Transactions on Image Processing*, vol. 25, no. 11, pp. 5187–5198, 2016.
- [6] H. Zhang and V. M. Patel, "Densely connected pyramid dehazing network," in *Proceedings of the IEEE conference on computer vision and pattern recognition*, 2018, pp. 3194–3203.
- [7] H. Zhang, V. Sindagi, and V. M. Patel, "Joint transmission map estimation and dehazing using deep networks," *IEEE Transactions on Circuits and Systems for Video Technology*, vol. 30, no. 7, pp. 1975–1986, 2019.
- [8] R. Li, J. Pan, Z. Li, and J. Tang, "Single image dehazing via conditional generative adversarial network," in *Proceedings of the IEEE Conference on Computer Vision and Pattern Recognition*, 2018, pp. 8202–8211.
- [9] Y. Qu, Y. Chen, J. Huang, and Y. Xie, "Enhanced pix2pix dehazing network," in *Proceedings of the IEEE Conference on Computer Vision and Pattern Recognition*, 2019, pp. 8160–8168.
- [10] X. Qin, Z. Wang, Y. Bai, X. Xie, and H. Jia, "Ffa-net: Feature fusion attention network for single image dehazing," in *AAAI*, 2020, pp. 11 908–11 915.
- [11] Y. Shao, L. Li, W. Ren, C. Gao, and N. Sang, "Domain adaptation for image dehazing," in *Proceedings of the IEEE/CVF Conference on Computer Vision and Pattern Recognition*, 2020, pp. 2808–2817.
- [12] R. Fattal, "Single image dehazing," *ACM transactions on graphics (TOG)*, vol. 27, no. 3, pp. 1–9, 2008.
- [13] —, "Dehazing using color-lines," *ACM transactions on graphics (TOG)*, vol. 34, no. 1, pp. 1–14, 2014.
- [14] W. Ren, S. Liu, H. Zhang, J. Pan, X. Cao, and M.-H. Yang, "Single image dehazing via multi-scale convolutional neural networks," in *European conference on computer vision*. Springer, 2016, pp. 154–169.
- [15] G. Wilson and D. J. Cook, "A survey of unsupervised deep domain adaptation," *ACM Transactions on Intelligent Systems and Technology (TIST)*, vol. 11, no. 5, pp. 1–46, 2020.
- [16] K. Bousmalis, N. Silberman, D. Dohan, D. Erhan, and D. Krishnan, "Unsupervised pixel-level domain adaptation with generative adversarial networks," in *Proceedings of the IEEE conference on computer vision and pattern recognition*, 2017, pp. 3722–3731.
- [17] A. Shrivastava, T. Pfister, O. Tuzel, J. Susskind, W. Wang, and R. Webb, "Learning from simulated and unsupervised images through adversarial training," in *Proceedings of the IEEE conference on computer vision and pattern recognition*, 2017, pp. 2107–2116.
- [18] J.-Y. Zhu, T. Park, P. Isola, and A. A. Efros, "Unpaired image-to-image translation using cycle-consistent adversarial networks," in *Proceedings of the IEEE international conference on computer vision*, 2017, pp. 2223–2232.
- [19] T. Kim, M. Cha, H. Kim, J. K. Lee, and J. Kim, "Learning to discover cross-domain relations with generative adversarial networks," *arXiv preprint arXiv:1703.05192*, 2017.
- [20] Z. Yi, H. Zhang, P. Tan, and M. Gong, "Dualgan: Unsupervised dual learning for image-to-image translation," in *Proceedings of the IEEE international conference on computer vision*, 2017, pp. 2849–2857.
- [21] C. Chen, W. Xie, W. Huang, Y. Rong, X. Ding, Y. Huang, T. Xu, and J. Huang, "Progressive feature alignment for unsupervised domain adaptation," in *Proceedings of the IEEE Conference on Computer Vision and Pattern Recognition*, 2019, pp. 627–636.
- [22] B. Sun and K. Saenko, "Deep coral: Correlation alignment for deep domain adaptation," in *European conference on computer vision*. Springer, 2016, pp. 443–450.
- [23] E. Tzeng, J. Hoffman, K. Saenko, and T. Darrell, "Adversarial discriminative domain adaptation," in *Proceedings of the IEEE conference on computer vision and pattern recognition*, 2017, pp. 7167–7176.
- [24] I. Goodfellow, J. Pouget-Abadie, M. Mirza, B. Xu, D. Warde-Farley, S. Ozair, A. Courville, and Y. Bengio, "Generative adversarial nets," in *Advances in neural information processing systems*, 2014, pp. 2672–2680.
- [25] J. Bao, D. Chen, F. Wen, H. Li, and G. Hua, "Cvae-gan: Fine-grained

- image generation through asymmetric training,” in *Proceedings of the IEEE International Conference on Computer Vision (ICCV)*, Oct 2017.
- [26] J. Yang, A. Kannan, D. Batra, and D. Parikh, “Lr-gan: Layered recursive generative adversarial networks for image generation,” *arXiv preprint arXiv:1703.01560*, 2017.
 - [27] C. H. Lin, C.-C. Chang, Y.-S. Chen, D.-C. Juan, W. Wei, and H.-T. Chen, “Coco-gan: generation by parts via conditional coordinating,” in *Proceedings of the IEEE International Conference on Computer Vision*, 2019, pp. 4512–4521.
 - [28] Y. Choi, M. Choi, M. Kim, J.-W. Ha, S. Kim, and J. Choo, “Stargan: Unified generative adversarial networks for multi-domain image-to-image translation,” in *Proceedings of the IEEE conference on computer vision and pattern recognition*, 2018, pp. 8789–8797.
 - [29] P. Isola, J.-Y. Zhu, T. Zhou, and A. A. Efros, “Image-to-image translation with conditional adversarial networks,” in *Proceedings of the IEEE conference on computer vision and pattern recognition*, 2017, pp. 1125–1134.
 - [30] T.-C. Wang, M.-Y. Liu, J.-Y. Zhu, A. Tao, J. Kautz, and B. Catanzaro, “High-resolution image synthesis and semantic manipulation with conditional gans,” in *Proceedings of the IEEE conference on computer vision and pattern recognition*, 2018, pp. 8798–8807.
 - [31] C.-Y. Lee, S. Xie, P. Gallagher, Z. Zhang, and Z. Tu, “Deeply-supervised nets,” in *Artificial intelligence and statistics*, 2015, pp. 562–570.
 - [32] D. Sun, A. Yao, A. Zhou, and H. Zhao, “Deeply-supervised knowledge synergy,” in *Proceedings of the IEEE Conference on Computer Vision and Pattern Recognition*, 2019, pp. 6997–7006.
 - [33] Z. Zhang, X. Zhang, C. Peng, X. Xue, and J. Sun, “Exfuse: Enhancing feature fusion for semantic segmentation,” in *Proceedings of the European Conference on Computer Vision (ECCV)*, 2018, pp. 269–284.
 - [34] A. Newell, K. Yang, and J. Deng, “Stacked hourglass networks for human pose estimation,” in *European conference on computer vision*. Springer, 2016, pp. 483–499.
 - [35] Y. Ganin and V. Lempitsky, “Unsupervised domain adaptation by back-propagation,” in *International conference on machine learning*. PMLR, 2015, pp. 1180–1189.
 - [36] B. Li, W. Ren, D. Fu, D. Tao, D. Feng, W. Zeng, and Z. Wang, “Benchmarking single-image dehazing and beyond,” *IEEE Transactions on Image Processing*, vol. 28, no. 1, pp. 492–505, 2019.
 - [37] A. Paszke, S. Gross, S. Chintala, G. Chanan, E. Yang, Z. DeVito, Z. Lin, A. Desmaison, L. Antiga, and A. Lerer, “Automatic differentiation in pytorch,” 2017.
 - [38] L. Bottou, “Large-scale machine learning with stochastic gradient descent,” in *Proceedings of COMPSTAT’2010*. Springer, 2010, pp. 177–186.
 - [39] D. P. Kingma and J. Ba, “Adam: A method for stochastic optimization,” *arXiv preprint arXiv:1412.6980*, 2014.
 - [40] W. Ren, L. Ma, J. Zhang, J. Pan, X. Cao, W. Liu, and M.-H. Yang, “Gated fusion network for single image dehazing,” in *Proceedings of the IEEE Conference on Computer Vision and Pattern Recognition*, 2018, pp. 3253–3261.
 - [41] X. Liu, Y. Ma, Z. Shi, and J. Chen, “Griddehazenet: Attention-based multi-scale network for image dehazing,” in *Proceedings of the IEEE International Conference on Computer Vision*, 2019, pp. 7314–7323.